



Design, synthesis and evaluation of ^{18}F -labeled bradykinin B1 receptor-targeting small molecules for PET imaging



Zhengxing Zhang^a, Hsiou-Ting Kuo^a, Joseph Lau^a, Silvia Jenni^a, Chengcheng Zhang^a, Jutta Zeisler^a, François Bénard^{a,b}, Kuo-Shyan Lin^{a,b,*}

^a Department of Molecular Oncology, BC Cancer Agency, 675 West 10th Avenue, Vancouver, BC V5Z 1L3, Canada

^b Department of Radiology, University of British Columbia, 950 West 10th Avenue, Vancouver, BC V5Z 4E3, Canada

ARTICLE INFO

Article history:

Received 20 May 2016

Revised 23 June 2016

Accepted 24 June 2016

Available online 27 June 2016

Keywords:

Bradykinin B1 receptor

Antagonist

Fluorine-18

Molecular imaging

Positron emission tomography

ABSTRACT

Two fluorine-18 (^{18}F) labeled bradykinin B1 receptor (B1R)-targeting small molecules, ^{18}F -Z02035 and ^{18}F -Z02165, were synthesized and evaluated for imaging with positron emission tomography (PET). Z02035 and Z02165 were derived from potent antagonists, and showed high binding affinity (0.93 ± 0.44 and 2.80 ± 0.50 nM, respectively) to B1R. ^{18}F -Z02035 and ^{18}F -Z02165 were prepared by coupling 2- ^{18}F fluoroethyl tosylate with their respective precursors, and were obtained in 10 ± 5 ($n = 4$) and $22 \pm 14\%$ ($n = 3$), respectively, decay-corrected radiochemical yield with $>99\%$ radiochemical purity. ^{18}F -Z02035 and ^{18}F -Z02165 exhibited moderate lipophilicity ($\text{Log}D_{7.4} = 1.10$ and 0.59 , respectively), and were stable in mouse plasma. PET imaging and biodistribution studies in mice showed that both tracers enabled visualization of the B1R-positive HEK293T::hB1R tumor xenografts with better contrast than control B1R-negative HEK293T tumors. Our data indicate that small molecule antagonists can be used as pharmacophores for the design of B1R-targeting PET tracers.

© 2016 Elsevier Ltd. All rights reserved.

Positron emission tomography (PET) is a highly sensitive and quantifiable molecular imaging modality that can detect distribution of a minimal amount (pM) of radiotracers in the body. The most widely used clinical PET tracer is ^{18}F -labeled 2-fluoro-2-deoxyglucose (^{18}F -FDG). As a close analog of glucose, ^{18}F -FDG is avidly taken up by cells with increased glucose needs, and is used for the diagnosis and prognosis of cancer, and to monitor response after treatment.^{1–3} However, ^{18}F -FDG is not suitable for detecting slow growing tumors that do not have enhanced glycolytic activity.³ Therefore, radiotracers targeting other cancer imaging biomarkers especially receptors of peptide growth factors such as bombesin and somatostatin are being actively developed and evaluated in the clinic.^{4–8}

The bradykinin B1 receptor (B1R), a G-protein coupled receptor, is overexpressed in a variety of cancers, but has minimal expression in normal tissues.⁹ The endogenous B1R ligands are [des-Arg⁹]bradykinin (Arg-Pro-Pro-Gly-Phe-Ser-Pro-Phe) and [des-Arg¹⁰]kallidin (Lys-[des-Arg⁹]bradykinin).¹⁰ Activation of B1R has been shown to promote proliferation and invasion of cancer cells, and to induce angiogenesis.^{11–14} Therefore, B1R antagonism has been proposed as a promising strategy for cancer

therapy.⁹ Effective B1R-targeting PET tracers could potentially be used to select patients who can benefit from emerging anti-B1R therapies. Previously, our group reported the evaluation of several potent radiolabeled [des-Arg¹⁰]kallidin derivatives for cancer imaging.^{15–18} Our data indicate that in vivo stability is crucial as only radiolabeled [des-Arg¹⁰]kallidin derivatives with unnatural amino acid substitutions in the peptide sequence were effective in visualizing B1R-expressing tumors.^{15–18} This is because the native [des-Arg¹⁰]kallidin peptide sequence can be rapidly degraded in vivo by peptidases.¹⁵

In addition to B1R-targeting peptides, a significant number of potent B1R small molecule antagonists have been developed by pharmaceutical companies for the treatment of chronic pain,^{19–23} and could potentially be exploited for the design of B1R-targeting PET tracers. An advantage of using small molecules as opposed to peptide sequence is their reduced metabolic lability. Barth et al. reported a series of 2-[2-[[[4-methoxy-2,6-dimethylphenyl]sulfonyl]methylamino]ethoxy]acetamide derivatives that are potent and selective B1R antagonists.¹⁹ Modification of the small *N*-alkyl group in some of those compounds was tolerable as **1–4** (Fig. 1) exhibited comparable high binding affinity to B1R.¹⁹ Based on this observation, we hypothesized that replacing the small *N*-alkyl group (methyl, ethyl or 2-propyl) in **1–4** with a 2-fluoroethyl group to generate Z02035 and Z02165 would retain comparable binding

* Corresponding author. Tel.: +1 604 675 8208; fax: +1 604 675 8218.

E-mail address: klin@bccrc.ca (K.-S. Lin).

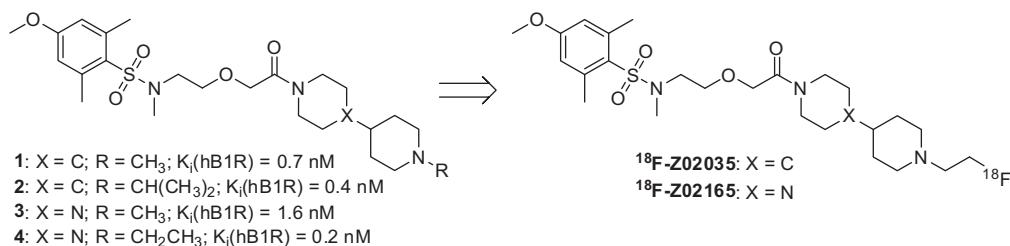


Figure 1. Design of ¹⁸F-labeled B1R-targeting tracers derived from small molecule antagonists.

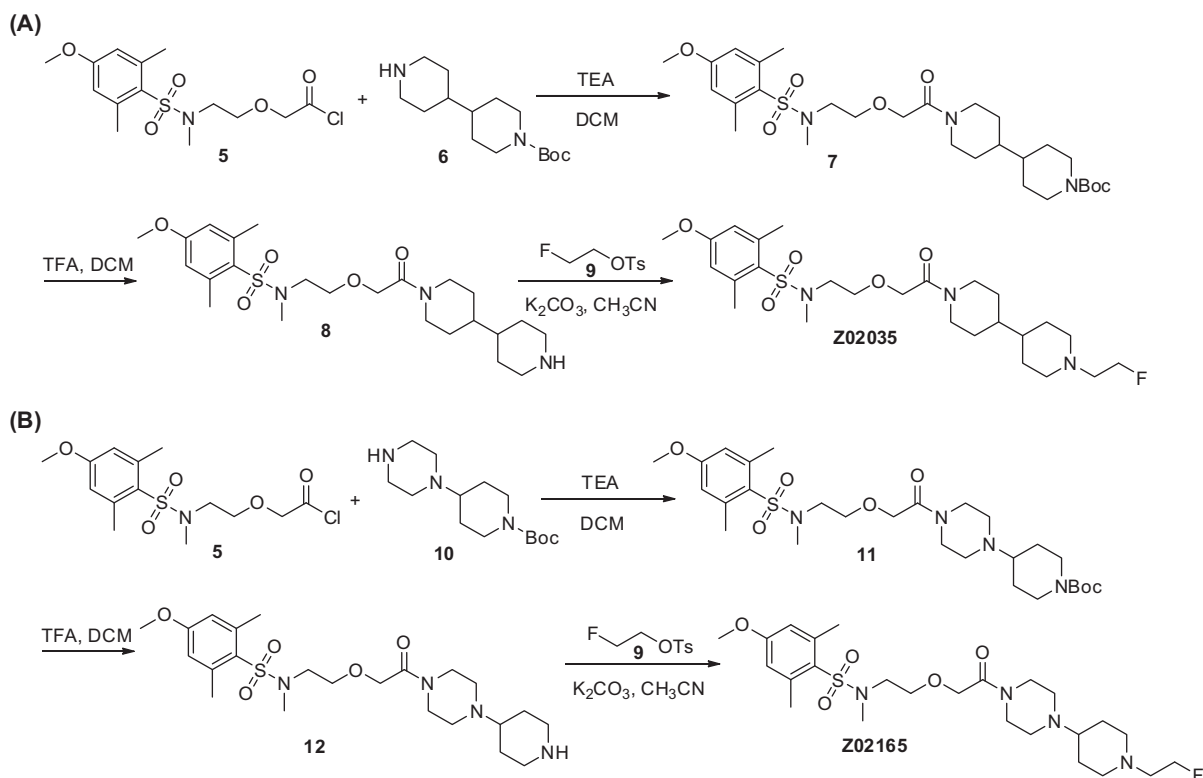
affinity to B1R. Since the fluorine atom at the 2-fluoroethyl group could be replaced with a radioactive ¹⁸F, the resultant ¹⁸F-labeled Z02035 and Z02165 could be exploited for PET imaging. In fact, replacing a methyl or ethyl group with a 2-[¹⁸F]fluoroethyl group is a common strategy to convert a potent therapeutic drug into a potential ¹⁸F-labeled PET imaging agent.^{24,25}

The syntheses of Z02035 and Z02165 are depicted in Scheme 1. For the synthesis of Z02035, 2-[2-[(4-methoxy-2,6-dimethylphenyl)sulfonyl]methylamino]ethoxy]acetyl chloride **5**²⁶ was first reacted with *N*-Boc-4,4'-bipiperidine **6**²⁷ in dichloromethane with triethylamine as the base to obtain **7** in 95% yield. The Boc protecting group was subsequently removed by treating **7** with trifluoroacetic acid, and the free amine **8** was isolated quantitatively. Coupling amine **8** with 2-fluoroethyl tosylate **9**²⁸ in acetonitrile with potassium carbonate as the base gave the cold standard Z02035 in 27% yield. The synthesis of Z02165 followed the same procedures for the synthesis of Z02035 but replacing *N*-Boc-4,4'-bipiperidine **6** with *tert*-butyl 4-piperazinotetrahydro-1(2*H*)-pyridinecarboxylate **10**. The Boc-protected intermediate **11**, free amine **12** and Z02165 were isolated in 83%, 100%, and 71% yields, respectively.

The binding affinities of Z02035 and Z02165 were measured via in vitro competition binding assays using B1R-expressing CHO-K1

cell membranes and [³H][Leu⁹,des-Arg¹⁰]kallidin as the radioligand.¹⁵ Both compounds inhibited the binding of [³H][Leu⁹,des-Arg¹⁰]kallidin to B1R in a dose dependant manner as shown in Figure 2. The K_i values for Z02035 and Z02165 are 0.9 ± 0.4 and 2.8 ± 0.5 nM, respectively. The low nM binding affinity values of Z02035 and Z02165 are comparable to those of compounds **1–4** (Fig. 1).¹⁹ This confirms our hypothesis that the small *N*-alkyl groups (methyl, ethyl, and 2-propyl) in **1–4** could be replaced with a 2-fluoroethyl group, and the resultant 2-fluoroethyl derivatives (Z02035 and Z02165) would still retain good binding affinity to B1R. As the binding affinities of Z02035 and Z02165 are comparable to those of previously reported radiolabeled B1R-targeting peptides,^{15–18} we proceeded with radiolabeling and imaging studies with Z02035 and Z02165.

¹⁸F-labeled Z02035 and Z02165 were prepared in two steps as shown in Scheme 2. The two-step approach was adopted to avoid the possibility of forming aziridinium in a one-step ¹⁸F-nucleophilic substitution reaction. First, a 2-[¹⁸F]fluoroethylation synthon was prepared followed by a coupling reaction with the respective amine precursors **8** and **12** to give the desired ¹⁸F-labeled Z02035 and Z02165, respectively. 2-[¹⁸F]Fluoroethyl tosylate (¹⁸F)**9** was chosen as it is the most widely used synthon for the 2-[¹⁸F]fluoroethylation reaction, and could be prepared



Scheme 1. Synthesis of (A) Z02035 and its radiolabeling precursor **8**; and (B) Z02165 and its radiolabeling precursor **12**.

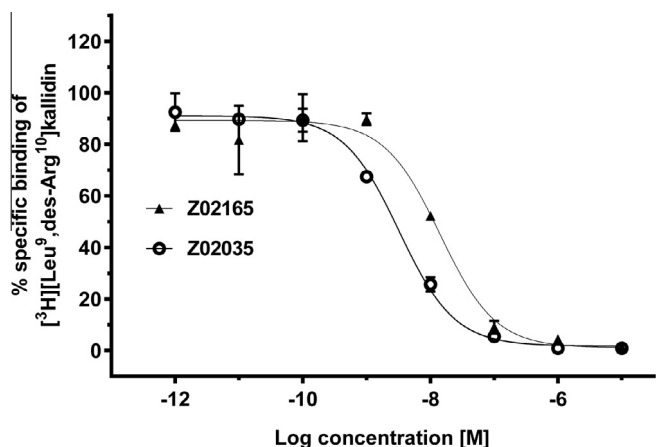


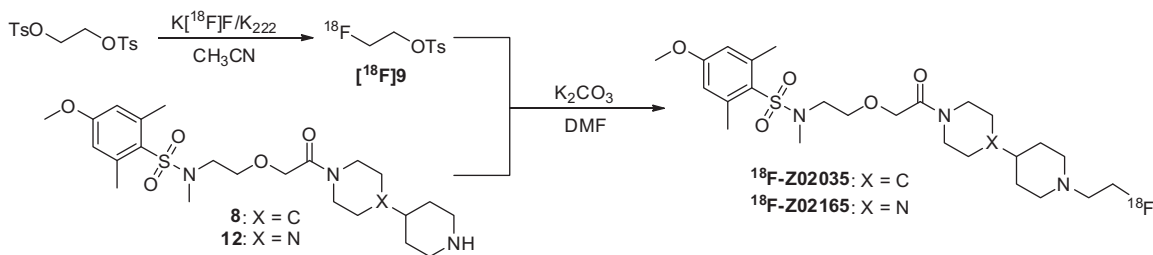
Figure 2. Representative displacement curves of [^3H]-[Leu 9 ,des-Arg 10]kallidin by Z02035 and Z02165.

efficiently as reported by incubating commercially available 1,2-bis(tosyloxy)ethane with $\text{K}[^{18}\text{F}]\text{F}/\text{K}_{222}$ in acetonitrile.²⁹ The subsequent coupling with the amine precursor **8** and **12** was conducted in *N,N*-dimethylformamide with potassium carbonate as the base. ^{18}F -Z02035 was isolated in $10 \pm 5\%$ ($n = 4$) decay-corrected radiochemical yield with $>99\%$ radiochemical purity and 38 ± 22 GBq/ μmol specific activity at the end of synthesis. For

^{18}F -Z02165, it was isolated in $22 \pm 14\%$ ($n = 3$) decay-corrected radiochemical yield with $>99\%$ radiochemical purity and 54 ± 33 GBq/ μmol specific activity at the end of synthesis.

The stability of ^{18}F -Z02035 and ^{18}F -Z02165 were evaluated in mouse plasma, and monitored by radio-HPLC. As shown in Figure 3, both ^{18}F -Z02035 and ^{18}F -Z02165 were relatively stable with 86% and 97% of the radiotracers remaining intact after being incubated in mouse plasma for 60 min. Log $D_{7.4}$ measurement was conducted using the shake flask method as previously reported to estimate tracer lipophilicity.¹⁵ Both tracers are moderately lipophilic and the Log $D_{7.4}$ values ($n = 3$) for ^{18}F -Z02035 and ^{18}F -Z02165 are 1.10 ± 0.08 and 0.59 ± 0.01 , respectively. Previously tested B1R-targeting peptides did not cross the blood–brain barrier due to their bulky size (>1500 Da) and high hydrophilicity (Log $D_{7.4} < -2.50$). With a smaller size (~ 500 Da) and moderate lipophilicity, ^{18}F -Z02035 and ^{18}F -Z02165 could potentially cross the blood–brain barrier and be used for imaging B1R expression in neurological disorders.^{30,31}

To evaluate the potential of ^{18}F -Z02035 and ^{18}F -Z02165 for imaging B1R expression, static/dynamic imaging and biodistribution studies were conducted in mice bearing both B1R-positive (B1R+) HEK293T::hB1R and B1R-negative (B1R-) HEK293T wild-type tumors. The B1R+ HEK293T::hB1R cells were created by transduction of the hB1R gene into wild-type HEK293T cells.¹⁵ Imaging mice bearing both B1R- HEK293T and B1R over-expressing HEK293T::hB1R tumors offers the advantage of verifying if the uptake in tumors is B1R mediated in a single study. This could be



Scheme 2. Radiosynthesis of ^{18}F -Z02035 and ^{18}F -Z02165.

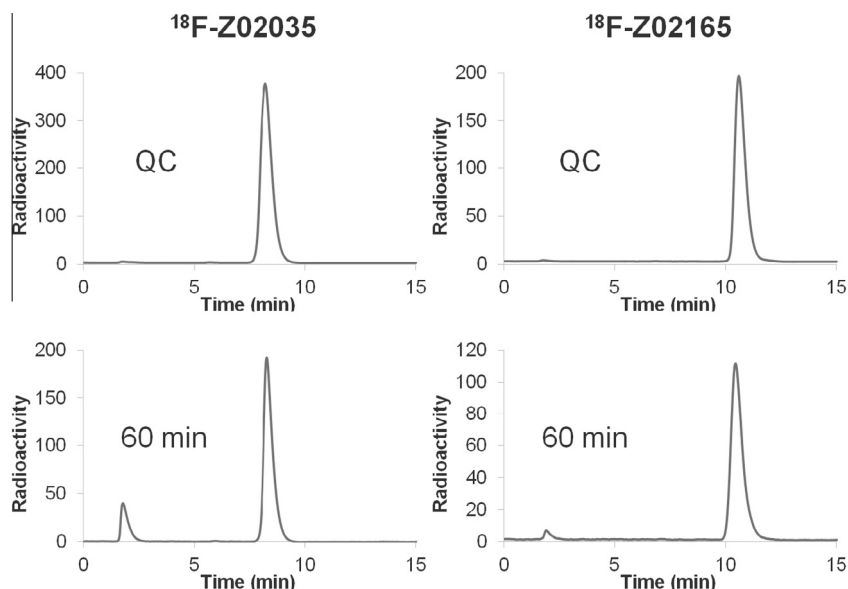


Figure 3. Radio-HPLC chromatograms of ^{18}F -Z02035 and ^{18}F -Z02165. Upper chromatograms: purified QC samples; lower chromatograms: extracted samples after being incubated with mouse plasma for 60 min.

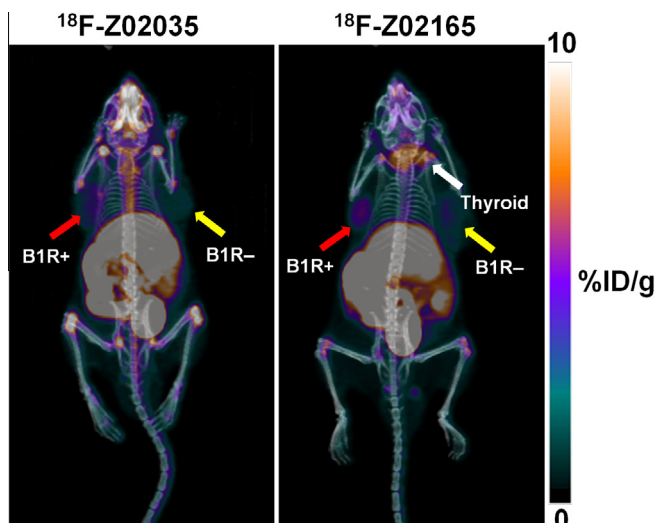


Figure 4. Maximum intensity projection images of ^{18}F -Z02035 (left) and ^{18}F -Z02165 (right) in mice bearing B1R+ HEK293T::B1R tumor (red arrow) and B1R– HEK293T wild-type tumor (yellow arrow). Thyroid is indicated by a white arrow. The 10-min static images were taken at 50–60 min post-injection.

performed by directly comparing the uptake difference between B1R– HEK293T and B1R+ HEK293T::hB1R tumors, and without blocking studies.

Representative static images of ^{18}F -Z02035 and ^{18}F -Z02165 acquired at 50–60 min post-injection interval are shown in

Figure 4. ^{18}F -Z02035 and ^{18}F -Z02165 were excreted via both renal and hepatobiliary pathways as high radioactivity accumulation was found in kidneys, bladder, liver and gut. Both tracers enabled visualization of the B1R+ HEK293T::hB1R tumors with better contrast than the B1R– HEK293T tumors. Uptake in some joints was detected especially when ^{18}F -Z02035 was used, indicating the occurrence of in vivo defluorination. The clear background (low muscle uptake) suggests no apparent defluoroethylation occurred as the ^{18}F -labeled defluoroethylated metabolites could significantly increase background activity level.^{32–34} An unexpected finding was the high uptake of ^{18}F -Z02165 in thyroid. However, this may not be B1R mediated because B1R expression level is low in normal tissues and no significant thyroid uptake was observed from our previous imaging studies using radiolabeled B1R-targeting [des-Arg¹⁰]kallidin derivatives.^{15–18} It is well documented that radiolabeled lipophilic cations such as $^{99\text{m}}\text{Tc}$ -sestamibi and ^{18}F -labeled phosphonium derivatives can be taken up by thyroid.^{35–37} With the amino group(s) in their structures ^{18}F -Z02035 and ^{18}F -Z02165 can form cationic protonated species at the physiological pH. It is, therefore, possible that the uptake of ^{18}F -Z02035 and ^{18}F -Z02165 in thyroid was due to the formation of their protonated species.

The time–activity curves of ^{18}F -Z02035 and ^{18}F -Z02165 derived from the dynamic imaging data are shown in **Figure 5**. The heart uptake (open blue circle) of both tracers peaked within the first two minutes to reach $\sim 18\% \text{ID/g}$, and dropped down to $< 3\% \text{ID/g}$ after 4-min post-injection, indicating fast clearance from the blood. The uptake in B1R+ tumors (solid red circle) was higher than that of B1R– tumors (open black triangle) at all time points, confirming specific binding of both tracers to B1R. High thyroid uptake ($\sim 7\%$

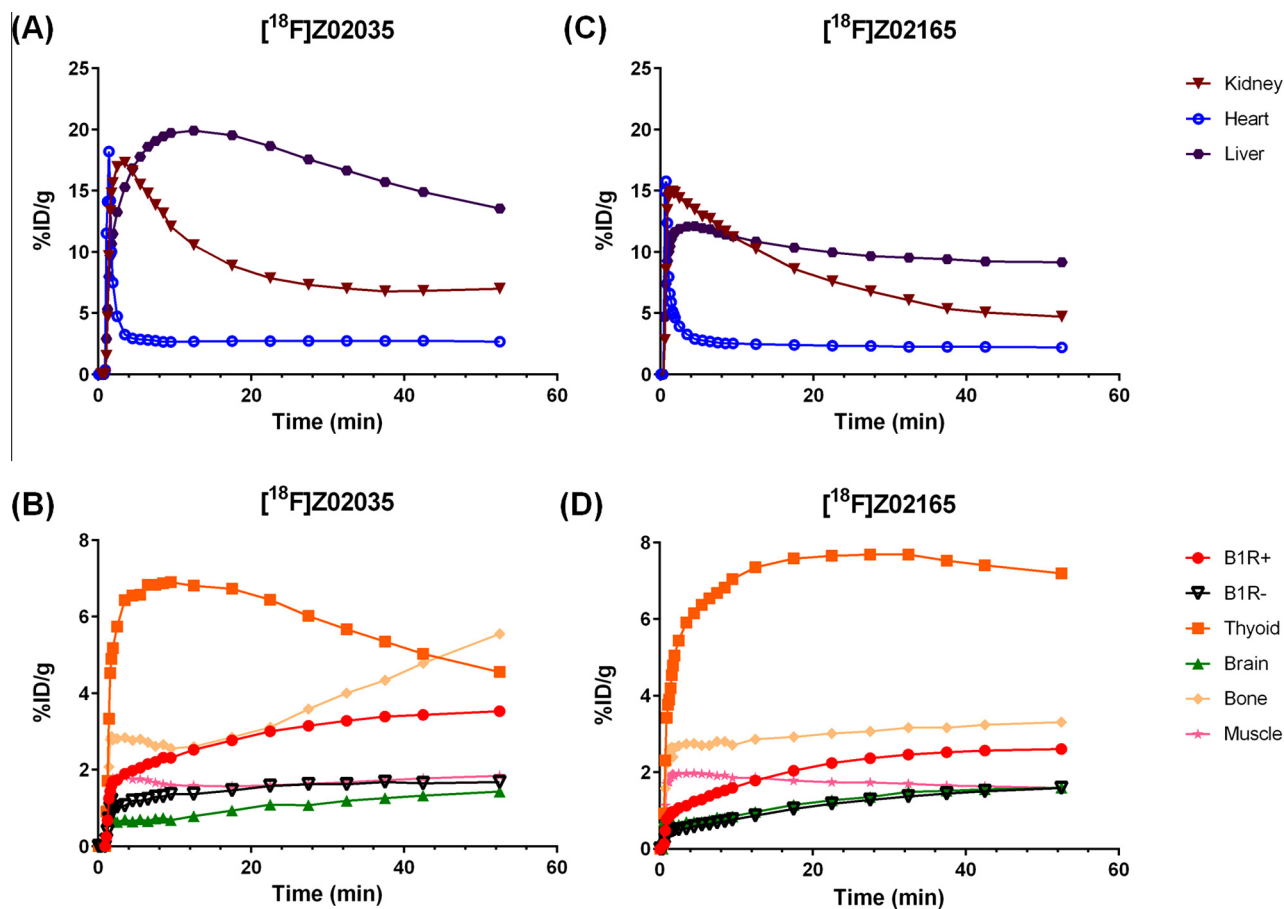


Figure 5. Time–activity curves of ^{18}F -Z02035 (A and B) and ^{18}F -Z02165 (C and D) in mice bearing B1R+ HEK293T::B1R tumor and B1R– HEK293T wild-type tumor.

Table 1

Biodistribution data (mean \pm SD, 1-h post-injection) of ^{18}F -Z02035 and ^{18}F -Z02165 in mice bearing both B1R+ HEK293T::hB1R and B1R– HEK293T tumors

Tissues/organs (%ID/g)	^{18}F -Z02035 (n = 6)	^{18}F -Z02165 (n = 5)
Blood	1.67 \pm 0.23	1.62 \pm 0.11
Fat	0.60 \pm 0.09	0.29 \pm 0.11***
Testes	1.00 \pm 0.11	1.11 \pm 0.15
Intestine	8.84 \pm 1.12	10.0 \pm 1.12
Stomach	4.75 \pm 1.56	3.29 \pm 1.22
Spleen	3.10 \pm 0.81	5.64 \pm 0.97***
Liver	10.1 \pm 1.63	8.17 \pm 0.55*
Pancreas	7.58 \pm 1.76	2.67 \pm 0.59***
Adrenal gland	1.68 \pm 0.26	1.73 \pm 0.50
Kidney	4.71 \pm 1.32	4.41 \pm 1.43
Lung	2.01 \pm 0.29	2.84 \pm 0.36**
Heart	1.67 \pm 0.23	1.65 \pm 0.14
Tumor(B1R+)	3.77 \pm 0.79	3.21 \pm 0.21
Tumor(B1R–)	2.11 \pm 0.37	1.98 \pm 0.17
Muscle	1.17 \pm 0.28	1.19 \pm 0.16
Bone	4.63 \pm 0.65	2.56 \pm 0.35***
Brain	0.80 \pm 0.08	1.06 \pm 0.08***
Tumor(B1R+)/tumor(B1R–)	1.78 \pm 0.17	1.65 \pm 0.20
Tumor/blood	2.26 \pm 0.35	1.99 \pm 0.22
Tumor/muscle	3.38 \pm 1.05	2.74 \pm 0.33

*, ** and *** indicate that the *p* value is <0.05, <0.01, or <0.001, respectively.

ID/g, solid orange square) was observed for both tracers. However, in static images (Fig. 4) it was more apparent by using ^{18}F -Z02165 due to the higher bone uptake level (solid beige diamond) of ^{18}F -Z02035. The bone uptake of ^{18}F -Z02035 increased continuously at later time points at a faster rate than that of ^{18}F -Z02165, suggesting ^{18}F -Z02035 is less stable against in vivo defluorination. The brain uptake (solid green triangle) of both tracers reached \sim 1%ID/g after 20 min post-injection. However, the observed slow increase of brain uptake for both tracers at later time points needs to be further verified. This could be simply due to the signal interference from the increasing skull uptake at later time points.

The results of biodistribution studies at 1-h post-injection are summarized in Table 1, and the data are consistent with observations from static images and time-activity curves. Higher uptake (\sim 8–10%ID/g) of both tracers was observed in intestines and livers. The high uptake (7.58 \pm 1.76%ID/g) of ^{18}F -Z02035 in pancreas was unexpected, and may not be B1R-mediated as no significant pancreas uptake was observed previously using radiolabeled peptide-based B1R-targeting tracers.^{15–18} Currently, the most widely used tracers for imaging pancreatic β -cell mass are radiolabeled dihydrotetrabenazine (DTBZ) derivatives targeting vesicular monoamine transporter 2 (VMAT2).^{38,39} There are some similarities between DTBZ and the core structure of ^{18}F -Z02035, and therefore the possibility for the uptake of ^{18}F -Z02035 into pancreas via VMAT2 cannot be ruled out. However, further studies are needed to confirm if the uptake of ^{18}F -Z02035 into pancreas is indeed mediated by VMAT2.

The bone uptake of ^{18}F -Z02035 (4.63 \pm 0.65%ID/g) was significantly (*p* < 0.001) higher than that of ^{18}F -Z02165 (2.56 \pm 0.35%ID/g), suggesting that ^{18}F -Z02035 is more prone to in vivo defluorination. The brain uptake values for ^{18}F -Z02035 and ^{18}F -Z02165 at 1-h post-injection were 0.80 \pm 0.08 and 1.06 \pm 0.08%ID/g, respectively. These uptake values were much higher than those (0.01–0.03% ID/g) obtained previously using radiolabeled peptide-based B1R-targeting tracers,^{15–18} confirming the ability of ^{18}F -Z02035 and ^{18}F -Z02165 to cross the blood–brain barrier. The uptake values of ^{18}F -Z02035 and ^{18}F -Z02165 in B1R+ HEK293T::hB1R tumors were 3.77 \pm 0.79 and 3.21 \pm 0.21%ID/g, respectively. These numbers were higher than their uptakes values in B1R– HEK293T tumors, blood and muscle. The uptake ratios of tumor(B1R+)-to-tumor(B1R–), tumor(B1R+)-to-blood and tumor(B1R+)-to-muscle are

1.78 \pm 0.17, 2.26 \pm 0.35 and 3.38 \pm 1.05, respectively for ^{18}F -Z02035, and 1.65 \pm 0.20, 1.99 \pm 0.22 and 2.74 \pm 0.33, respectively for ^{18}F -Z02165. No significant difference was observed by comparing the uptake in B1R+ tumor as well as the uptake ratios of tumor(B1R+)-to-tumor(B1R–), tumor(B1R+)-to-blood and tumor(B1R+)-to-muscle between ^{18}F -Z02035 and ^{18}F -Z02165 (Table 1). This implies that both tracers perform equally well for the detection of B1R expression in tumors.

In conclusion, we took a novel approach for imaging B1R expression by exploiting the potential of two ^{18}F -labeled small molecules, ^{18}F -Z02035 and ^{18}F -Z02165. Although tumor-to-background contrast ratios are lower than those of reported B1R tracers derived from peptide sequences, both ^{18}F -Z02035 and ^{18}F -Z02165 were able to differentiate between B1R expressing and non-expressing tumor xenografts. Due to advantages of brain penetration and in vivo stability against peptidase degradation, small molecule pharmacophores are promising for use for the design of B1R-targeting PET tracers. Optimization to enhance tumor uptake/contrast and to reduce in vivo defluorination and non-specific binding is currently underway.

Acknowledgements

This work was supported by the Canadian Institutes of Health Research (MOP-126121). The authors would like to thank Milan Vuckovic, Wade English, Julius Klug, Nadine Colpo and Navjit Hundal-Jabal for their technical assistance.

Supplementary data

Supplementary data associated with this article can be found, in the online version, at <http://dx.doi.org/10.1016/j.bmcl.2016.06.066>.

References and notes

- Smith, G.; Carroll, L.; Aboagye, E. O. *Mol. Imaging Biol.* **2012**, *14*, 653.
- Jadvar, H.; Alavi, A.; Gambhir, S. J. *Nucl. Med.* **2009**, *50*, 1820.
- Fletcher, J. W.; Djulbegovic, B.; Soares, H. P.; Siegel, B. A.; Lowe, V. J.; Lyman, G. H.; Coleman, R. E.; Wahl, R.; Paschold, J. C.; Avril, N.; Einhorn, L. H.; Suh, W. W.; Samson, D.; Delbeke, D.; Gorman, M.; Shields, A. F. *J. Nucl. Med.* **2008**, *49*, 480.
- Inkster, J.; Lin, K.-S.; Ait-Mohand, S.; Gosselin, S.; Bénard, F.; Guérin, B.; Pourghiasian, M.; Ruth, T.; Schaffer, P.; Storr, T. *Bioorg. Med. Chem. Lett.* **2013**, *23*, 3920.
- Li, Y.; Liu, Z.; Harwig, C. W.; Pourghiasian, W.; Lau, J.; Lin, K.-S.; Schaffer, P.; Bénard, F.; Perrin, D. M. *Am. J. Nucl. Med. Mol. Imaging* **2013**, *3*, 57.
- Liu, Z.; Pourghiasian, M.; Bénard, F.; Pan, J.; Lin, K.-S.; Perrin, D. M. *J. Nucl. Med.* **2014**, *55*, 1499.
- Pourghiasian, M.; Liu, Z.; Pan, J.; Colpo, N.; Lin, K.-S.; Perrin, D. M.; Bénard, F. *Bioorg. Med. Chem.* **2015**, *23*, 1500.
- Fani, M.; Maecke, H. R.; Okarvi, S. M. *Theranostics* **2012**, *2*, 481.
- da Costa, P. L. N.; Sirois, P.; Tannock, I. F.; Chamma, R. *Cancer Lett.* **2014**, *345*, 27.
- Leeb-Lundberg, L. M. F.; Marceau, F.; Muller-Esterl, W.; Pettibone, D. J.; Zuraw, B. L. *Pharmacol. Rev.* **2005**, *57*, 27.
- Barki-Harrington, L.; Bookout, A. L.; Wang, G.; Lamb, M. E.; Leeb-Lundberg, L. M. F.; Daaka, Y. *Biochem. J.* **2003**, *371*, 581.
- Molina, L.; Matus, C. E.; Astroza, A.; Pavicic, F.; Tapia, E.; Toledo, C.; Perez, J. A.; Nualart, F.; Gonzalez, C. B.; Burgos, R. A.; Figueroa, C. D.; Ehrenfeld, P.; Poblete, M. T. *Breast Cancer Res. Treat.* **2009**, *118*, 499.
- Lu, D. Y.; Leung, Y. M.; Huang, S. M.; Wong, K. L. *J. Cell Biochem.* **2010**, *110*, 141.
- Parenti, A.; Morbidelli, L.; Ledda, F.; Granger, H. J.; Ziche, M. *FASEB J.* **2001**, *15*, 1487.
- Lin, K.-S.; Pan, J.; Amouroux, G.; Turashvili, G.; Mesak, F.; Hundal-Jabal, N.; Pourghiasian, M.; Lau, J.; Aparicio, S. J.; Bénard, F. *Cancer Res.* **2015**, *75*, 387.
- Lin, K.-S.; Amouroux, G.; Pan, J.; Zhang, Z.; Jenni, S.; Lau, J.; Hundal-Jabal, N.; Colpo, N.; Bénard, F. *J. Nucl. Med.* **2015**, *56*, 622.
- Liu, Z.; Amouroux, G.; Zhang, Z.; Pan, J.; Hundal-Jabal, N.; Colpo, N.; Perrin, D. M.; Bénard, F.; Lin, K.-S. *Mol. Pharmaceutics* **2015**, *12*, 974.
- Amouroux, G.; Pan, J.; Jenni, S.; Zhang, C.; Zhang, Z.; Hundal-Jabal, N.; Colpo, N.; Liu, Z.; Bénard, F.; Lin, K.-S. *Mol. Pharmaceutics* **2015**, *12*, 2879.
- Barth, M.; Bondoux, M.; Luccarini, J.-M.; Peyrou, V.; Dodey, P.; Pruneau, D.; Massardier, C.; Paquet, J.-L. *J. Med. Chem.* **2012**, *55*, 2574.
- Huszar, J.; Timar, Z.; Bogar, F.; Penke, B.; Kiss, R.; Szalai, K. K.; Schmidt, E.; Papp, A.; Keseru, G. *J. Pept. Sci.* **2009**, *15*, 423.

21. Qian, W.; Chen, J. J.; Human, J.; Aya, T.; Zhu, J.; Biswas, K.; Peterkin, T.; Hungate, R. W.; Arik, L.; Johnson, E.; Kumar, G.; Joseph, S.; Jona, J.; Guo, H.-X.; Wu, Z. *Bioorg. Med. Chem. Lett.* **2012**, *22*, 1061.
22. Kuduk, S. D.; Bock, M. G. *Curr. Top. Med. Chem.* **2008**, *8*, 1420.
23. Liu, Q.; Qian, W.; Li, A.; Biswas, K.; Chen, J. J.; Fotsch, C.; Han, N.; Yuan, C.; Arik, L.; Biddlecome, G.; Johnson, E.; Kumar, G.; Lester-Zeiner, D.; Ng, G. Y.; Hungate, R. W.; Askew, B. C. *Bioorg. Med. Chem. Lett.* **2010**, *20*, 4593.
24. Lin, K.-S.; Ding, Y.-S. *Chirality* **2004**, *16*, 475.
25. Lin, K.-S.; Ding, Y.-S.; Kim, S. W.; Kil, K. E. *Nucl. Med. Biol.* **2005**, *32*, 415.
26. Merla, B.; Oberboersch, S.; Jostock, R.; Engels, M.; Schunk, S.; Reich, M.; Hees, S. U.S. Patent 2009/0186899.
27. Melchiorre, C.; Bolognesi, M. L.; Budriesi, R.; Ghelardini, C.; Chiarini, A.; Minarini, A.; Rosini, M.; Tumiatti, V.; Wade, E. J. *J. Med. Chem.* **2001**, *44*, 4035.
28. Wilson, A. A.; DaSilva, J. N.; Holsem, S. *Appl. Radiat. Isot.* **1995**, *46*, 765.
29. Riss, P. J.; Hoehnemann, S.; Piel, M.; Roesch, F. *J. Labelled Compd. Radiopharm.* **2013**, *56*, 356.
30. Passos, G. F.; Medeiros, R.; Cheng, D.; Vasilevko, V.; LaFerla, F. M.; Cribbs, D. H. *Am. J. Pathol.* **2013**, *182*, 1740.
31. Ongali, B.; Campos, M. M.; Bregola, G.; Rodi, D.; Regoli, D.; Thibault, G.; Simonato, M.; Couture, R. *J. Comp. Neurol.* **2003**, *461*, 506.
32. Pan, J.; Pourghasian, M.; Hundal, N.; Lau, J.; Benard, F.; Dedhar, S.; Lin, K.-S. *Nucl. Med. Biol.* **2013**, *40*, 850.
33. Zhang, Z.; Lau, J.; Kuo, H. T.; Zhang, C.; Hundal-Jabal, N.; Colpo, N.; Bénard, F.; Lin, K.-S. *Bioorg. Med. Chem. Lett.* **2016**, *26*, 584.
34. Pan, J.; Lau, J.; Mesak, F.; Hundal, N.; Pourghasian, M.; Liu, Z.; Bénard, F.; Dedhar, S.; Supuran, C. T.; Lin, K.-S. *J. Enzyme Inhib. Med. Chem.* **2014**, *29*, 249.
35. Smith, J. R.; Oates, M. E. *Radiographics* **2004**, *24*, 1101.
36. Zhang, Z.; Jenni, S.; Zhang, C.; Merkens, H.; Lau, J.; Liu, Z.; Perrin, D. M.; Bénard, F.; Lin, K.-S. *Bioorg. Med. Chem. Lett.* **2016**, *26*, 1675.
37. Wells, L.; Haslop, A.; Coello, C.; Keat, N.; Gee, A.; Passchier, J.; Long, N.; Plisson, C. *J. Nucl. Med.* **2014**, *55*, 121.
38. Simpson, N. R.; Souza, F.; Witkowski, P.; Maffei, A.; Raffo, A.; Herron, A.; Kilbourn, M.; Jurewicz, A.; Herold, K.; Liu, E.; Hardy, M. A.; Van Heertum, R.; Harris, P. E. *Nucl. Med. Biol.* **2006**, *33*, 855.
39. Kung, M.-P.; Hou, C.; Lieberman, B. P.; Oya, S.; Ponde, D. E.; Blankemeyer, E.; Skovronsky, D.; Kilbourn, M. R.; Kung, H. F. *J. Nucl. Med.* **2008**, *49*, 1171.